New CFD-based method for erosion prediction in control valves

Stefano Malavasi, Gianandrea V. Messa
Politecnico di Milano, Italy

Abstract

Control valves often experience erosion produced by the impacts of solid particles within the flow. This is a very serious concern of engineers, as it causes downtime, loss of income, and high repair costs. Field and lab erosion testing are extremely onerous both economically and technically and, for this reason, the use of CFD techniques for erosion prediction is gaining ground in recent years. The standard practice involves the usage of two-phase CFD models which follow the trajectories of all solid particles within the flow. However, the huge computational burden of these models even for simple flows prevents, or even preclude, their application to complex flows of engineering interest such as valve flows. In this paper an innovative approach for erosion prediction is proposed. Its strength compared to the traditional practice resides in the numerical efficiency, arising from the usage of a different CFD two-phase method in which the detailed analysis of the fluid dynamics characteristics of the solid particles is restricted to the vicinity of the surfaces most vulnerable to erosion. This feature reduces considerably the computational burden of the erosion predictions in case of simple flows and, most important, makes it feasible to perform these estimations also in case of complex geometries such as control valves. In this paper, we discuss about the application of the method to sketched model of a Needle and Seat valve after its validation in abrasive jet benchmark tests.

Introduction

The impact erosion, i.e. the loss of material caused by the impingements of solid particles dragged by a fluid, is a very serious concern in many engineering applications. This issue is very relevant in the oil&gas industry, because the extracted fluids are commonly accompanied by solids, typically sand, having considerable erosive potential. All hydraulic singularities present in the plants are particularly vulnerable to erosion through the induced

distortion of the flow field; among them, the choke valves used to control the flow on the risers. Particularly, the most important erosion-related problems are the identification of the erosion hotspot locations and the estimation of the loss of material from the valve under aggressive flow conditions. However, it is the latter which matters the most, the former being typically an issue only for the design of new devices. For existing valves, in fact, most manufacturers are already capable in identifying the parts of the trim which are most vulnerable to wear on the grounds of their experience.

Performing field and lab erosion testing for providing the erosion characterization of a control valve is extremely hard due to economic and technical difficulties, and only very few examples are mentioned in the literature [1-5]. For these reason, disposing of tools for erosion prediction is of considerable interest for engineers in the design stage as well as in the management one.
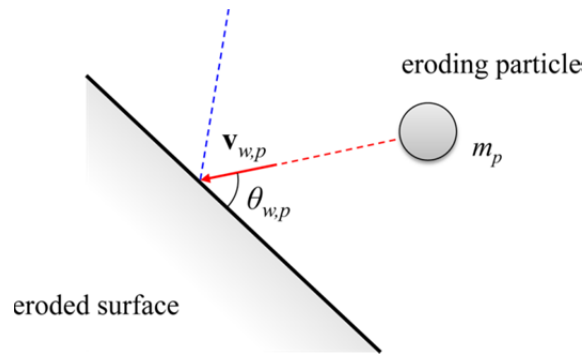

Fig. 1. An eroding particle hitting a surface.

At present, the standard practice involves the use of "single-particle" erosion correlations, which treat the erosion process in terms of the interaction between each eroding particle and a surface, and express the mass of eroded material removed E_p as a function of the particle mass m_p, the modulus of the particle impact speed vector $|\mathbf{v}_{p,w}|$, the particle impact angle $\theta_{w,p}$, and some properties of the materials involved in the erosion process (Fig. 1). Typically the erosion correlations are of empirical nature and are obtained by fitting the outcomes of laboratory tests in which an abrasive jet impinges at high velocity against a specimen of the target material, even if this practice is still one of the most restricting uncertainties in erosion prediction [3]. In this work we will employ the DNV erosion correlation [6], one of the most commonly used in the oil&gas industry. This equation is as follows:

$$E_p = m_p K \left| \mathbf{v}_{p,w} \right|^n F\left(\theta_{w,p}\right) \qquad F\left(\theta_{w,p}\right) = \sum_{i=1}^{8} A_i \theta_{w,p}^i \qquad (1)$$

where K and n are constants depending on the material and the A_i coefficients are given in [6].

The fluid dynamic properties of the particles at the impact stage, $|\mathbf{v}_{p,w}|$ and $\theta_{w,p}$, are usually obtained from CFD simulations based on the Eulerian-Lagrangian (EL) approach under the assumption of "one-way coupling" regime, in which the fluid flow without solids is first simulated in an Eulerian framework (i.e. cell-based), and, afterwards, the solid phase is represented in a Lagrangian framework by tracking the trajectories of a certain number of parcels (i.e. group of particles sharing the same fluid-dynamic properties). This approach provides rather accurate estimates of the two-phase flow field, but it is extremely onerous from a computational point of view. In fact, since the computed trajectories are random due to the dispersive action of the fluid turbulence, many parcels have to be tracked in order to have significant erosion rate statistics. The number of sample trajectories required, which is considerable even for simple geometries, is of the order of tens of thousands for valve flow simulations [3,7]. This leads to a huge amount of calculated data, most of which are completely useless for the erosion prediction purposes. Just to give an idea, storing the position and the velocity of all the 100.000 parcels tracked in our Eulerian-Lagrangian simulation would require about 30 GB disk space. Moreover, the already high computational burden of the EL models becomes prohibitive when:

1) the solid loading exceeds a certain value (say 0.1% by volume), because the assumption of "one-way coupling" regime does not hold anymore and the parcels' trajectories have to be iteratively recalculated in order to account for their influence on the fluid phase motion as well as the possible interactions among the particles themselves. As far as we know, no attempt of predicting the valve erosion produced by dense mixtures has been reported in the literature except for a relatively recent study in which the geometry of the device had been extremely simplified and modeled as two-dimensional [8].

2) the change in the valve geometry due to erosion is significant and the flow has to be modeled as unsteady or quasi-steady like in the work by Nguyen et al. [9]. However, a model accounting geometry changes dynamically does not seem to be available at present.

The literature available indicates that, when applied to valves, the approach reported above is capable in reproducing the erosion hotspot locations but fails in predicting correctly the amount of removed material [3,5], and this has been mainly attributed to the employment of inadequate erosion correlations as well as the neglect of the geometry changes due to erosion. The high computational burden is another drawback that must also be considered, because it may become a limiting factor when trying to account for geometry changes as well as addressing dense flows.

In this work we focus precisely on this last limitation, presenting a new methodology which allows restricting the amount of calculated data regarding the particle properties to just a portion of the computational domain in the proximity of the erosion hotspot locations. This is achieved by combining the tracking of the parcels' trajectories with an Eulerian-Eulerian two-phase CFD model which solves only for the average properties of the ensemble of particles. Here we had necessarily to refer to a simplified situation in order to have the possibility to compare our model with the standard EL-based practice, which is inapplicable to a real case due to its excessive computational burden. However, with the proposed methodology the most restrictive assumptions (i.e. simplified valve model, "one-way coupling" regime, and fixed valve geometry) can be overcome. Therefore we will be able to address erosion prediction on a real design, taking in account of geometry changes due to erosion and considering both diluted and dense flows.
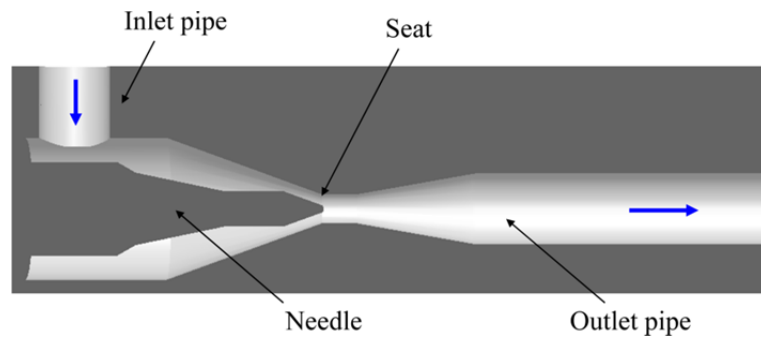

Fig. 2. A section of the sketched "Needle and Seat" valve considered in this study.

The remainder of this paper is divided in three sections, followed by the conclusions. The mathematical models are first described, together with the numerical setup and the computational methodology. The new approach is then illustrated and, afterwards, applied to the prediction of erosion in a sketched model of a 25 mm (2 in) "Needle and Seat" valve, shown in Fig. 2.

Mathematical models

In this research we made use of the Eulerian-Lagrangian and the Eulerian-Eulerian CFD models embedded in the PHOENICS code version 2011. However, it is worth noticing that the used models, which are described in detail in [10] and whose main features are briefly reported in the following, are the typical ones that are available in the other general-purpose CFD codes; therefore, we would expect similar results to be produced by other codes. We

also underline that the proposed methodology is applicable regardless of the specific two-phase CFD model and erosion correlation used.

Eulerian-Lagrangian modelling

As already noticed, due to the low solid loading considered in this preliminary study the Eulerian-Lagrangian (EL) simulations were performed under the hypothesis of "one-way coupling" regime, in which the fluid affects the motion of the particles but not vice-versa. Therefore, the fluid flow field is obtained from single-phase flow computations by solving the steady-state RANS equations coupled with the standard k-ε turbulence model. Solution of these equations yields the mean velocity vector of the fluid $\mathbf{U}_{EL}$, the mean pressure of the fluid P_{EL}, the turbulent kinetic energy k_{EL}, and its dissipation rate ε_{EL}.

Under the hypothesis that the parcels do not interact with each other, the Lagrangian tracking calculations are performed by solving the following set of ordinary differential equation for each parcel:

$$\begin{cases} \dfrac{d\mathbf{x}_{EL}}{dt} = \mathbf{v}_{EL} \\[2mm] \dfrac{d\mathbf{v}_{EL}}{dt} = \dfrac{3}{4d_p}\dfrac{\rho_f}{\rho_p}C_d\left|\tilde{\mathbf{u}}_{EL}-\mathbf{v}_{EL}\right|\left(\tilde{\mathbf{u}}_{EL}-\mathbf{v}_{EL}\right)+\dfrac{1}{\rho_p}\tilde{\nabla}P_{EL} \end{cases} \tag{2}$$

where $\mathbf{x}_{EL}$ is the parcel position vector, $\mathbf{v}_{EL}$ is the instantaneous parcel velocity vector, d_p is the particle diameter, C_d is the drag coefficient, ρ_f and ρ_p are the densities of fluid and particles respectively, and the tilde symbol indicates that the instantaneous fluid velocity $\mathbf{u}^{EL}$ and the gradient of the mean fluid pressure ∇P_{EL} are evaluated at parcel position. The drag coefficient C_d is evaluated from the local particle Reynolds number by means of the correlation of Clift et al. [11]. Other forces, such as gravity, Saffman lift, Magnus lift, virtual mass, and history force, were neglected being apparently related to side effects of minor importance for the case study under consideration. The stochastic turbulence model of Gosman and Ioannides [12] was employed for the evaluation of the instantaneous fluid velocity vector $\mathbf{u}_{EL}$.

Eulerian-Eulerian modelling

In the Eulerian-Eulerian approach both phases are interpreted as interpenetrating continua and the average fluid dynamic properties of the ensemble of particles, referred to as "solid phase" are solved in an Eulerian, cell-based framework. Particularly, the model of Spalding [13]

embedded in the PHOENICS code and employed in this study solves the following set of steady-state mass and momentum conservation equations for the fluid and the solid phases, respectively:

$$\nabla \cdot \left[\rho_f \left(1 - \Phi_{EE} \right) \mathbf{U}_{EE} \right] - \nabla \cdot \left(\rho_f \overline{\phi'_{EE} \, \mathbf{u}'_{EE}} \right) = 0 \tag{3}$$

$$\nabla \cdot \left(\Phi_{EE} \rho_p \mathbf{V}_{EE} \right) + \nabla \cdot \left(\rho_p \overline{\phi'_{EE} \, \mathbf{v}'_{EE}} \right) = 0 \tag{4}$$

$$\nabla \cdot \left[\rho_f \left(1 - \Phi_{EE} \right) \mathbf{U}_{EE} \mathbf{U}_{EE} \right] - \nabla \cdot \left[\left(1 - \Phi_{EE} \right) \left(\mu + \mu_{EE}^t \right) \nabla \mathbf{U}_{EE} \right] = \\ + \nabla \cdot \left(\rho_f \overline{\phi'_{EE} \, \mathbf{u}'_{EE}} \mathbf{U}_{EE} \right) = - \left(1 - \Phi_{EE} \right) \nabla P_{EE} + \mathbf{M}_{EE} \tag{5}$$

$$\nabla \cdot \left(\rho_p \Phi_{EE} \mathbf{V}_{EE} \mathbf{V}_{EE} \right) - \nabla \cdot \left(\Phi_{EE} \mu_{EE}^t \nabla \mathbf{V}_{EE} \right) - \nabla \cdot \left(\rho_p \overline{\phi'_{EE} \, \mathbf{v}'_{EE}} \mathbf{V}_{EE} \right) = - \Phi_{EE} \nabla P_{EE} - \mathbf{M}_{EE} \tag{6}$$

where: Φ_{EE} and ϕ'_{EE} are the mean and fluctuating solid volume fraction; $\mathbf{U}_{EE}$ and $\mathbf{u}'_{EE}$ are the mean and fluctuating fluid velocity vectors; $\mathbf{V}_{EE}$ and $\mathbf{v}'_{EE}$ are the mean and fluctuating velocity vectors of the solid phase; P_{EE} is the mean pressure, shared by the phases; μ and μ^t are the viscosity of the fluid and the eddy viscosity respectively; and $\mathbf{M}_{EE}$ is the generalized drag term, which accounts for the momentum transfer between the phases. For consistency with the EL simulations, $\mathbf{M}_{EE}$ includes only the drag force and it is therefore given by:

$$\mathbf{M}_{EE} = \frac{3}{4 d_p} \rho_f \Phi_{EE} C_d \left| \mathbf{U}_{EE} - \mathbf{V}_{EE} \right| \left(\mathbf{U}_{EE} - \mathbf{V}_{EE} \right) \tag{7}$$

with the drag coefficient evaluated by means of the correlation of Clift et al. [11].

The correlations between the fluctuating velocity and the fluctuating volume fractions are modeled by means of the eddy diffusivity hypothesis, as follows

$$\overline{\phi'_{EE} \, \mathbf{u}'_{EE}} = \overline{\phi'_{EE} \, \mathbf{v}'_{EE}} = \frac{\mu_{EE}^t}{\rho_f \sigma_\Phi} \nabla \Phi_{EE} \tag{8}$$

where σ_Φ is the turbulent Schmidt number for volume fractions, which is assigned a unit value in this work. The eddy viscosity μ_{EE}^t is obtained by means of a two-phase extension of the standard k-ε turbulence model, embedded in PHOENICS and described in [10].

Computational domain and boundary conditions
The computational domain in shown in Fig. 3. The geometrical symmetry of the valve with respect to the mid plane could not be exploited by solving only over half of the device because of the strong swirl occurring in the valve body and the downstream pipe, a very

6

critical feature in valve flow simulations [14]. At the inlet section, in both the EL and EE simulations the fluid axial velocity was uniformly distributed, whilst the turbulent kinetic energy and its dissipation rate were derived from a turbulent intensity of 5% and an inlet mixing length equal to 7% of the pipe diameter. In the EL simulations, the initial position of each parcel is obtained by random sampling from a uniform PDF on the boundary, whilst the inlet parcel velocity $\mathbf{v}_{EL,in}$ and its mass flow rate $\dot{m}_P$ were set as follows

$$\mathbf{v}_{EL,in} = \tilde{\mathbf{U}}_{EL,in} + \xi \left(\frac{2\tilde{k}_{EL,in}}{3} \right)^{1/2} \qquad \dot{m}_P = \rho_p A_P C \left(\tilde{\mathbf{U}}_{EL,in} \cdot \mathbf{n} \right) \qquad (9)$$

where $\mathbf{U}_{EL,in}$ and $k_{EL,in}$ are the mean velocity vector and the turbulent kinetic energy of the fluid at the inlet section, ξ is a three-element vector containing random scalars drawn from the standard PDF, C is the average inlet solid volume fraction, $\mathbf{n}$ is the normal unit vector to the inlet boundary, and A_P is an equivalent parcel area determined in such a way that the total solid mass flux entering the domain is constant regardless of the number of tracked parcels. In the EE simulations, at the inlet section the mean velocity vector of the solid phase is set equal to that of the fluid, and the inlet solid volume fraction is set as uniform. The short inlet pipe length simulated ($1D$) does not allow attaining fully-developed flow conditions at the valve entrance, but this is unlikely to have any effect on the two-phase flow field within the valve body, thereby affecting the quality of our erosion estimates.
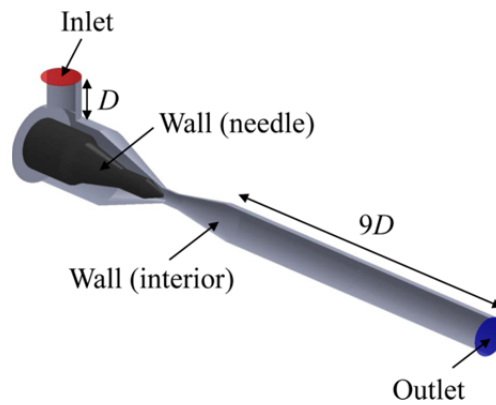

Fig. 3. Computational domain and boundary conditions.

At the outlet boundary the mean pressure is specified and held constant to a zero value. In the EL simulations, the parcels simply leave the domain, whilst in the EE ones the solid volume fraction and mass outflow of the solid phase result as part of the overall solution. The

outlet section is located 9*D* downstream the valve body in order to allow a complete pressure recovery.

At the wall boundaries (which includes the surfaces of the needle, the chamber, the seat, and the upstream and downstream pipes), no slip is assumed for the fluid phase, and the equilibrium wall function of Launder and Spalding [15] is employed for evaluating the fluid wall shear stress, and the turbulent kinetic energy and its dissipation rate in the near-wall cells. In the EL simulations, the normal and tangential components of the reflected parcel velocity are related to the corresponding incident values via two restitution coefficients, both set to a unit value. In the EE simulations, a zero wall shear stress condition has been applied to the solid phase at solid walls.

Computational methodology and consistency of the numerical solution

The single-phase RANS and the EE equations have been discretized using the finite volume method, and the calculations performed following the elliptic-staggered formulation. Central differencing is employed for the diffusion terms, while the convection terms are discretized using the hybrid differencing scheme of Spalding [16]. The finite volume equations are solved iteratively by means of the SIMPLEST [17] and IPSA [13] algorithms of Spalding. Inertial relaxation is applied to the momentum equations with a false-time step of 0.01 s, and a linear relaxation factor of 0.4 is applied to all other flow variables.

A structured mesh in Cartesian coordinates is used to discretize the domain, and the PARSOL immersed-boundary method [10] is employed to detect the solid boundaries. The mesh used consisted of 4.7 million cells, the grid being densified within the valve body. A grid independence study was performed to guarantee the consistency of the numerical solution. Particularly, the flow simulation was repeated employing three different grids in which the number of cells was increased from 1.1 to 4.7 million, and it was investigated the effect of the number of cells upon the flow coefficient C_V defined as:

$$C_V = Q\sqrt{\frac{\rho_f / \rho_{f,0}}{\Delta P}} \tag{10}$$

where Q is the volume flow rate expressed in gallon per minute (gpm), $\rho_{f,0}$ is the fluid density at a temperature of 15°C, and ΔP is the pressure drop expressed in pounds per square inches (psi), evaluated as the difference between the mean pressure at the inlet section and that at a distance of 6*D* downstream the diffuser. The results, shown in Fig. 4(a), reveal that as the number of cells increases the predicted C_V approaches a constant value, which is the same for

both the EL and EE simulations. Therefore, the mesh uses proved capable in providing consistent estimation of the flow coefficient, indicating the ability to correctly predict the acceleration effects that influence the erosion conditions directly.
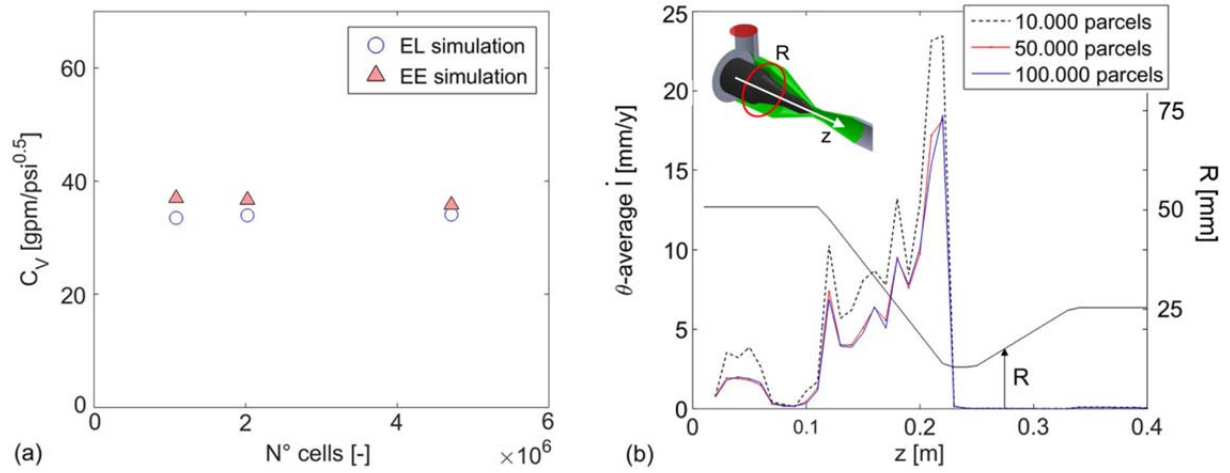

Fig. 4. (a) Effect of the number of cells on the flow coefficient predictions; (b) Effect of the number of parcels upon the average penetration rate over outer-wall circumferences.

Owing to the assumption of "one-way coupling" regime, the parcels' equations are integrating after the solution of the fluid flow field. This is done by means of the GENTRA package version 2010 embedded in the PHOENICS code, supplied by user-made FORTRAN coding allowing the parcels' impact data to be stored. Extensive MATLAB routines have been also developed for the post-processing of the GENTRA output. Particularly, the valve surface has been triangulated and each impact point has been associated to the nearest centroid of the surface elements. Application of the erosion correlation (Eq. 1) in which the particle mass m_p had been replaced by the parcel mass flux $\dot{m}_P$ yields the mass flux of eroded material removed by the current parcel. The sum over the parcels yields the erosion rate of each surface element, which, once divided by the product of the surface element area and the wall density, produces the local penetration rate, $\dot{I}$ (mm/year).

Since each parcel is associated a mass flux $\dot{m}_P$ (given by Eq. 9), the erosion at the walls due to individual parcels' impacts is therefore related to the mass flux that each parcel represents. In order to insure that a statistically representative set of particle impingements are obtained, the effect of the number of parcels on the predicted erosion rate is investigated. Particularly, the number of tracked parcels is increased from 10000 to 100000 and it is analyzed the effect of such variation upon the penetration rate distribution on the outer wall which, at each axial location, is evaluated as the average value of $\dot{I}$ over the corresponding

9

outer-wall circumference. The results, reported in Fig. 4(b), confirm the significance of the statistics obtained on a sample of 100000 trajectories. Releasing such a number of parcels leads to huge amount of calculated data which, as already said, would require about 30 GB disk space to be stored. Nevertheless, only a small portion of all this information is really needed for erosion prediction. This consideration has been the starting point for developing the proposed methodology, which will be illustrated in the following section.

The proposed method

The idea at the basis of the new method is to perform a Lagrangian tracking of the parcels' trajectories only in subsets of the computational domain (referred to as Ω subdomains) closed to the wear hotspot locations, thereby determining the parcels' characteristics only where it matters from the point of view of erosion prediction. In order to find the parcels' trajectories within the Ω subdomains, the following quantities must be known: 1) the fluid flow field with in Ω; 2) the boundary conditions for the parcels. All the required information is obtained from an EE simulation, which provides the average properties of the fluid and the solid phases.
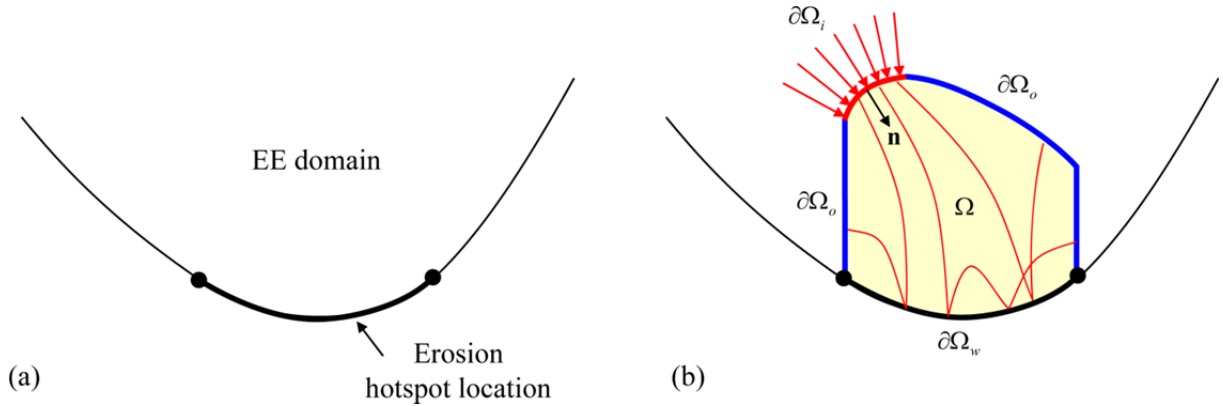

Fig. 5. (a) The EE domain and an erosion hotspot location (b) An Ω subdomain and its boundaries.

Particularly, the following steps are to be taken. An EE simulation is first performed, and the average properties of the fluid and the solid phase (i.e. $\mathbf{U}_{EE}$, $\mathbf{V}_{EE}$, P_{EE}, and Φ_{EE}) are determined in the whole computational domain (Fig. 5(a)). Afterwards, the Ω-subdomains (Fig. 5(b)) are identified as it will be discussed later in this section. The parcels' trajectories are then determined within Ω by integrating a system of ordinary differential equations which is analogous to Eq. (2), with the only difference that the fluid properties are obtained from the EE simulation (i.e. $\mathbf{u}_{EL}$ and P_{EL} are replaced by $\mathbf{u}_{EE}$ and P_{EE} respectively; $\mathbf{u}_{EE}$ is again evaluated using the stochastic method of Gosman and Ioannides [12]).

The boundary conditions for the parcels are specified as follows. The border of Ω will consists of one or more inlet boundaries $\partial\Omega_i$, outlet boundaries $\partial\Omega_o$, and wall boundaries $\partial\Omega_w$. The boundary conditions on $\partial\Omega_o$ and $\partial\Omega_w$ are specified as in the EL simulations, i.e. the parcels leave Ω through $\partial\Omega_o$ and, on $\partial\Omega_w$, the normal and tangential components of the reflected parcel velocity are related to the corresponding incident values via two restitution coefficients. The parcels' properties on $\partial\Omega_i$ are instead obtained from the outcomes of the EE simulation. This is done by identifying on $\partial\Omega_i$ a set of fixed positions where the parcels will be released; the number of parcels introduced at each position will be proportional to the area specific mean solid mass flux obtained from the EE simulation, i.e. $\rho_p \tilde{\Phi}_{EE} \tilde{\mathbf{V}}_{EE} \cdot \mathbf{n}$ (again, $\mathbf{n}$ is the local unit inward normal to $\partial\Omega_i$, and a tilde symbol indicates that Φ_{EE} and $\mathbf{V}_{EE}$ are interpolated at parcel position). The inlet parcel velocity $\mathbf{v}_i$ and its mass flow rate $\dot{m}_P$ were set as:

$$\mathbf{v}_i = \tilde{\mathbf{V}}_{EE} + \boldsymbol{\xi}\left(\frac{2\tilde{k}_{EE}}{3}\right)^{1/2} \qquad \dot{m}_P = \frac{A_P}{\dfrac{\tilde{\mathbf{V}}_{EE}}{\left|\tilde{\mathbf{V}}_{EE}\right|}\cdot\mathbf{n}}\left[\rho_p\tilde{\Phi}_{EE}\left|\tilde{\mathbf{V}}_{EE}\right| - \frac{\tilde{\mu}_{EE}^t}{\sigma_\Phi}\left(\tilde{\nabla}\tilde{\Phi}_{EE}\cdot\mathbf{n}\right)\right]\cdot\mathbf{n} \qquad (11)$$

where, as in the EL simulations, $\boldsymbol{\xi}$ is a three-element vector containing random scalars drawn from the standard PDF, and A_P is an equivalent parcel area determined in such a way that the total solid mass flux entering Ω is constant regardless of the number of tracked parcels.

As already observed in the "Introduction", the identification of the erosion hotspots locations (and, therefore, the definition of the Ω subdomains) may not be an issue since they could be already known on the basis of experience. However, if no information is available at all, gross localization of the surfaces most exposed to wear can be identified by tracking a small number of parcels within the entire flow domain after performing the EE simulation. It is worth noticing that this calculation will have little effect on the computational gain of using the proposed method; in fact, the high computational burden of the EL computations mainly arise from the considerable number of trajectories necessary to achieve reliable statistics, but only a limited number of trajectories (around 1000 in our simulations, but this value is expected to be problem-dependent) are needed to understand with sufficient accuracy where the erosion hotspots locations are. Once they are identified, and so the $\partial\Omega_w$ boundaries are, the Ω subdomains can be defined, bearing in mind that the smaller their size is, the greater the reduction of the computational burden is. Actually, the only constrain is that the inlet

boundary $\partial\Omega_i$ must not be too close to the wall in order to avoid possible inconsistency in the application of the interfacial laws (Eq. 11).

Application

As already noticed, in order to be able to compare the proposed methodology with the standard EL-based predictive method, we had to consider only dilute flows under the assumption of "one-way coupling" regime, and neglect the geometry changes due to erosion. The results obtained at this stage will open the way for removing these hypotheses in future research.

Before applying the methodology described in the previous subsection to the "Needle and Seat" valve sketched in Fig. 2, extensive work has been devoted at validating the method in a simpler flow, namely the normal impingement of an abrasive jet against a surface. We will now briefly report the outcome of this study, certainly not intending to be exhaustive.
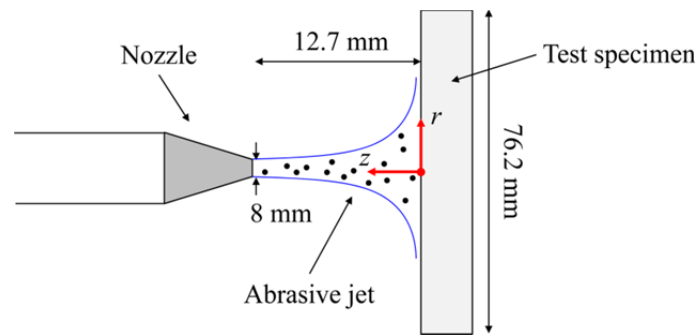

Fig. 6. The abrasive jet validation test.

The case, which reproduces the laboratory tests of Okita et al. [18], is shown in Fig. 6. The carrier fluid is water and the jet is submerged, and the average jet velocity is 10 m/s. The nozzle diameter is 8 mm, and the distance between the nozzle exit and the test specimen (which is a cylinder with diameter 76.2 mm) is 12.7 mm. The solid phase consists of spherical particles with size of 120 μm and density of 2700 kg/m^3. The average solid volume fraction at the nozzle exit is 1‰.

The flow has been modeled as 2D axisymmetric for computational speed. First, an EE simulation was performed and the release of 1000 parcels at the inlet section allowed defining the Ω subdomain shown in Fig. 7(a) and its boundaries $\partial\Omega_i$, $\partial\Omega_o$, $\partial\Omega_w$, and $\partial\Omega_a$, the last one being an axis of symmetry. Afterwards, the parcels' trajectories were calculated only within Ω and the initial characteristics deduced from the interfacial laws (Eq. 11). The radial distribution of the penetration rate $\dot{I}$ was then calculated by dividing the specimen radius in

intervals of size 0.5 mm, and the resulting profile was then compared against the one obtained from a EL simulation performed in the whole domain. In both simulations, 50.000 trajectories were sufficient to provide statistically significant erosion predictions.
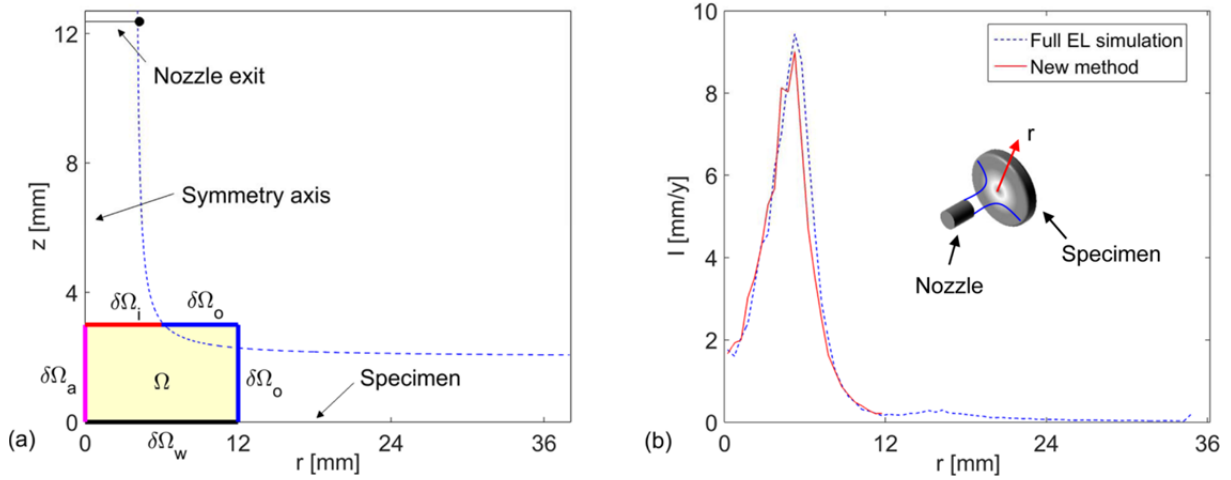

Fig. 7. (a) The Ω subdomain and its boundaries (b) Radial distribution of the penetration rate.

The results are shown in Fig. 7(b), and clearly reveal that the maximum erosion occurs somewhere further from the symmetry axis, in agreement with the findings of previous experiments [9]. The small discrepancies between the two curves confirm the reliability of the proposed methodology. In order to quantify the gain of employing the new method instead of performing a full EL simulation, reference is made to the space on disk needed to store all the computed data (i.e. the Eulerian variables in all computational cells and the position and velocity of all parcels at each Lagrangian time step), even if not all this information has actually to be stored for erosion analysis. In this simple two-dimensional case under the hypothesis of "one-way coupling" regime, the disk space required would be around 3 GB, about 60% lower compared to the 7.5 GB needed by a full EL simulation. All the data stored in the extra 4.5 GB disk space was completely useless for erosion prediction.

The "Needle and Seat" valve depicted in Fig. 2 will be now addressed. Particularly, we considered the following flow conditions: water flow rate in the 2" inlet pipe = 14.2 l/s (average velocity = 7 m/s); particle density = 2700 kg/m^3; particle diameter = 400 μm; and average solid volume fraction at the inlet section = 1‰. Details of the numerical setup, including flow domain, boundary conditions, and computational methodology, have already been given.

We applied the proposed methodology by following the steps illustrated in the previous subsection. First of all, we simulated the solid-liquid flow within the device using the EE

model, thereby determining the average properties of the two phases and the mean solid volume fraction in each computational cell (Fig. 8(a)).
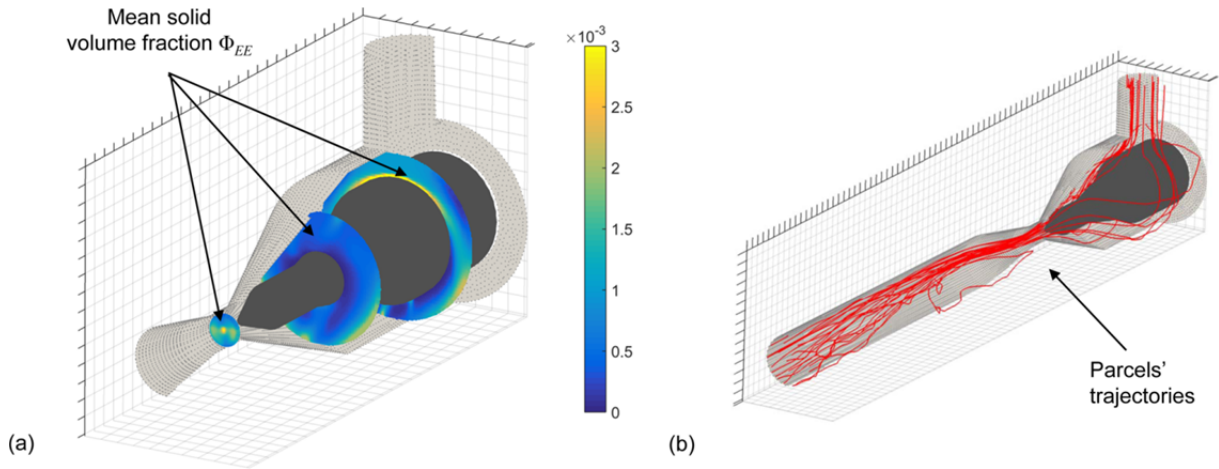

Fig. 8. (a) Crosswise distributions of the mean solid volume fraction Φ_{EE} as obtained from the EE simulation; (b) Some representative parcels' trajectories used for defining the Ω subdomain.
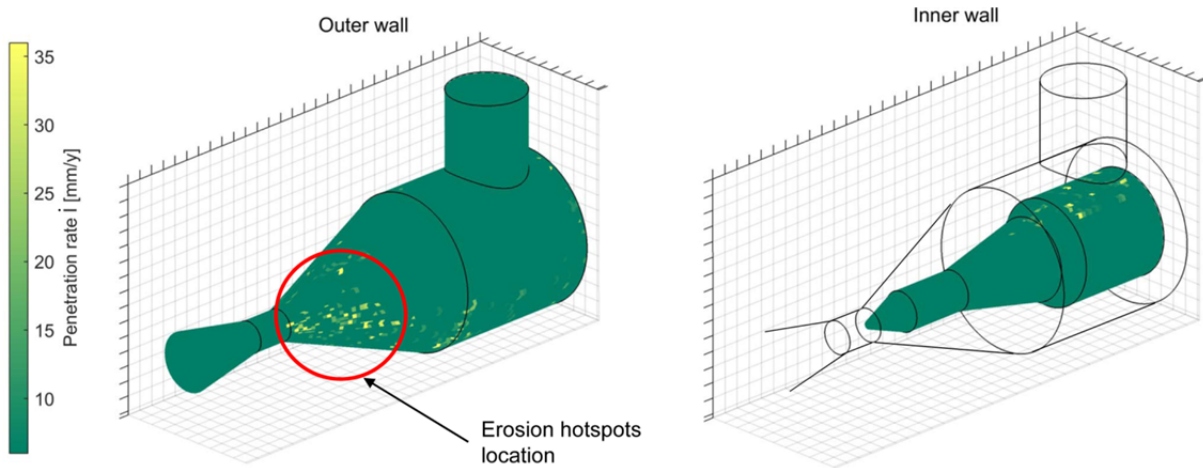

Fig. 9. Penetration rate distribution over the valve surface as obtained from the injection of 1000 testing parcels through the inlet boundary.

Afterwards, we identified the hotspots locations, thereby determining the Ω subdomain. This was achieved by injecting 1000 parcels through the inlet section (the trajectories of 20 out them are shown in Fig. 8(b)) and then evaluating the penetration rate distribution over the valve surface. The outcomes of this analysis, shown in Fig. 9, indicate that even if 1000 parcels are too few to obtain statistically significant values of penetration rate, they are sufficient to clearly understand that erosion will affect the outer chamber in correspondence of

the reducer upstream the seat. Based on these results, we defined a possible Ω subdomain of interest, which is shown in Fig. 10 together with its boundaries $\partial\Omega_i$, $\partial\Omega_o$, and $\partial\Omega_w$. As already noticed, strong swirl occurred within the valve, resulting in asymmetrical distributions of mean velocity and mean solid volume fraction. For this reason, the Ω subdomain spanned over the whole angular extension of the reducer.
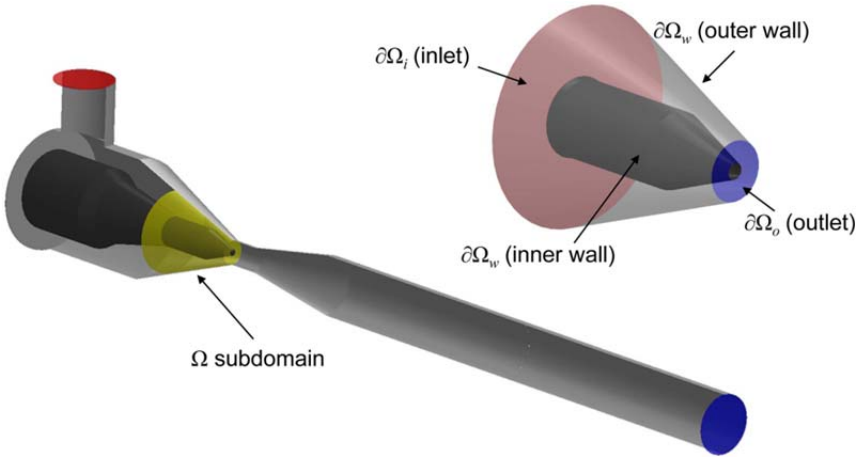

Fig. 10. The Ω subdomain and its boundaries $\partial\Omega_i$, $\partial\Omega_o$, and $\partial\Omega_w$.
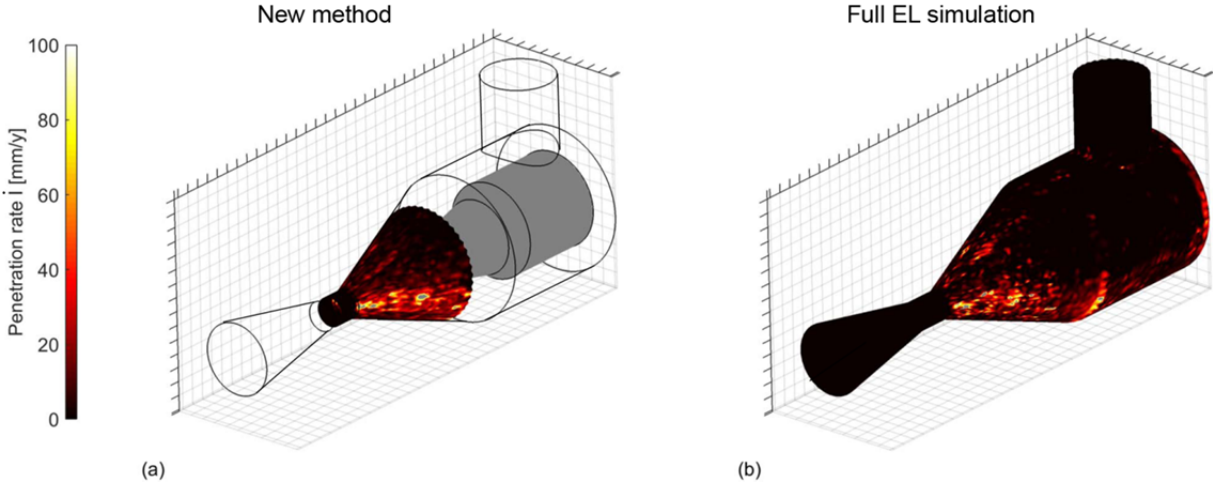

Fig. 11. Penetration rate distribution as obtained from: (a) the new method; (b) a full EL simulation.

The trajectories of 100000 parcels were tracked within Ω, after obtaining their characteristics at the inlet section $\partial\Omega_i$ from the interfacial laws (Eq. 11). The penetration rate distribution was then calculated over the outer wall boundary, and depicted in Fig. 11(a). A similar plot is shown in Fig. 11(b) for a full EL simulation. The two solutions show

similarities and, in both cases, the maximum wear occurs opposite to the inlet pipe. In explaining the differences, one should also consider that 100000 parcels could be not enough to attain statistically stable distributions of local penetration rate, since such analysis has been performed only with respect to the average value of $\bar{i}$ over outer-wall circumferences. In Fig. 12 the erosion rate is quantified with respect to this integral parameter, and the outcomes of the new methodology are in qualitative agreement and quantitatively comparable with a full EL simulation.
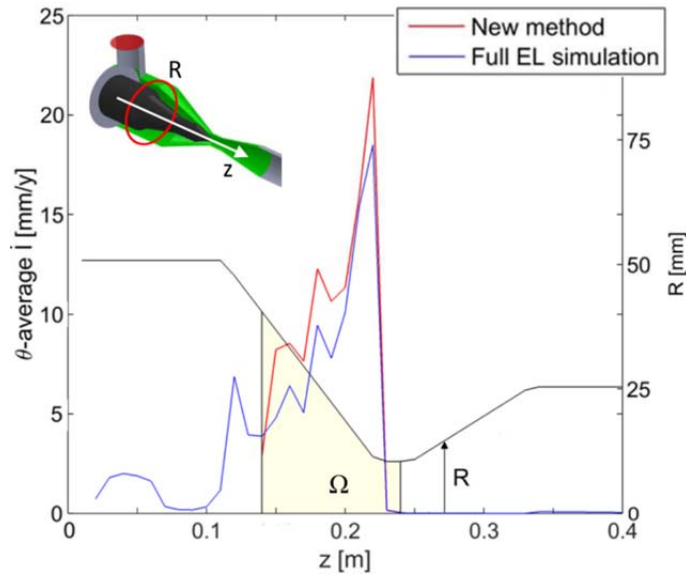

Fig. 12. Average penetration rate over outer-wall circumferences: comparison between the new method and a full EL simulation. The radial profile of the outer wall is shown and labeled on the right vertical axis.

Also in this complex case, and always under the assumption of "one-way coupling" regime, the gain is considerable when using the new method. In fact, the disk space which is virtually needed to store all the computed information would reduce from 30 GB to 7 GB, because 21 GB of useless information are not computed with the new method.

If, now, attention is paid to the obtained erosion predictions, it can be observed from Fig. 12 that the simulated flow conditions produce significant penetration rates which will cause within a short time severe damage to the valve or at least loss of flow control capacity. However, the present case study is a typical example of flows in which accounting for the geometry changes due to erosion is necessary to provide more accurate long-term erosion rate predictions. At present this appears difficult (and sometimes impossible) to achieve with the

16

standard EL-based practice, but the reduction of the computational burden made possible by the proposed method will allow addressing this issue in future research.

Conclusion

An innovative methodology allowed reducing the computational burden of the CFD-based erosion prediction analyses which usually rely on Eulerian-Lagrangian two-phase flow simulations. This is particularly important since the high computational burden is one of the main limitations of the practice commonly followed at present, and it may even preclude its applicability to non-dilute flows as well as the possibility to account for geometry changes due to erosion.

The basic idea of the proposed methodology is to perform the tracking of the parcels' trajectories only in subsets of the computational domain located in the proximity of the erosion hotspot locations, which may be either already known on the basis of experience or easily obtained with relatively low computational effort. The parcels' trajectories in the subsets are determined starting from the output of an Eulerian-Eulerian two-phase flow simulation, which consists in the mean fluid-dynamic characteristics of the fluid and of the ensemble of particles. The new method avoids computing large amount of data which are completely ineffective from the point of view of erosion prediction.

The proposed methodology has been applied successfully to a benchmark test regarding the normal impingement of an abrasive jet against a specimen of an eroding material (Fig. 6) and, afterwards, to a sketched model of a "Needle and Seat" valve (Fig. 2). In both cases, the new method proved capable in providing estimates of the hotspots penetration rates which are very close to those obtained from a full Eulerian-Lagrangian simulation but with about 60% less computed data (Fig. 7(b) and 12). The reduction of the computational burden made will make it possible to address denser flows as well as accounting dynamically for geometry change effects.

Nomenclature

A_i coefficients in Eq. (1) (-)

A_P equivalent parcel area (m^2)

C average solid volume fraction at the inlet section (-)

C_d drag coefficient (-)

C_V valve flow coefficient ($gpm/psi^{0.5}$)

D pipe diameter (m)

d_p diameter of a particle (m)

E_p mass of eroded material removed per impact (kg)

$\dot{I}$ penetration rate (mm/y)

K coefficient in Eq. (1) (s^n/m^n)

k turbulent kinetic energy (m^2/s^2)

$\mathbf{M}$ generalized drag (N/m^3)

$\dot{m}_P$ mass flow rate of a parcel (kg/s)

m_p mass of a particle (kg)

$\mathbf{n}$ normal unit vector pointing inward (-)

n coefficient in Eq. (1) (-)

P mean pressure (Pa)

Q flow rate (gpm)

R radius of valve chamber

r radial coordinate

z axial coordinate

$\mathbf{U}$ mean velocity vector of the fluid (m/s)

$\mathbf{u}$ instantaneous velocity vector of the fluid (m/s)

$\mathbf{u}$'   fluctuating velocity vector of the fluid (m/s)

t Lagrangian time (s)

$\mathbf{V}$ mean velocity vector of the solid phase (m/s)

$\mathbf{v}_{p,w}$ particle impact velocity vector (m/s)

$\mathbf{v}$ instantaneous velocity vector of a parcel (m/s)

$\mathbf{v}$'   fluctuating velocity vector of the solid phase (m/s)

$\mathbf{x}$ position vector of a parcel (m)

ΔP pressure drop through the valve (psi)

ε dissipation rate (m^2/s^3)

θ angular coordinate (rad)

$\theta_{w,p}$ particle impact angle (-)

μ viscosity of the fluid (Ns/m^2)

μ^t eddy viscosity (Ns/m^2)

ξ random vector drawn from the standard PDF (-)

ρ_f density of the fluid (kg/m^3)

$\rho_{f,0}$ density of the fluid at a temperature of 15°C (kg/m^3)

ρ_p density of the particles (kg/m^3)

σ_Φ turbulent Schmidt number for volume fractions (-)

Φ mean volume fraction of the solid phase (-)

ϕ' fluctuating volume fraction of the solid phase (-)

Ω subdomain

$\partial\Omega_a$ axis boundary of Ω

$\partial\Omega_i$ inlet boundary of Ω

$\partial\Omega_o$ outlet boundary of Ω

$\partial\Omega_w$ wall boundary of Ω

Superscripts and subscripts

EE   obtained from an Eulerian-Eulerian simulation

EL   obtained from an Eulerian-Lagrangian simulation

in   at the inlet section

References

[1]. Haugen, R., Kvernvold, O., Ronold, A., and Sandberg, R., 1995, Sand erosion of wear-resistant materials: Erosion in choke valves, Wear, 186-187, pp. 179-188.

[2]. Nokleberg, L., and Søntvedt, T., 1998, Erosion of oil&gas industry choke valves using computational fluid dynamics and experiment, Int. J. Heat Fluid Flow, 19, pp. 636-643.

[3]. Wallace, M.S., Dempster, W.M., Scanlon, T., Peters, J., and McCulloch, S., 2004, Prediction of impact erosion in valve geometries, Wear, 256, pp. 927-936.

[4]. Wheeler, D.W., Wood, R.J.K., Harrison, D., and Smith, E., 2006, Application of diamond to enhance choke valve life in erosive duties, Wear, 261, pp. 1087-1094.

[5]. Gharaibah, E., Zhang, Y., Paggiaro, R., and Friedemann, J., 2013, Prediction of Sand Erosion in Choke Valves – CFD Model Development and Validation Against Experiments, OTC Offshore Technology Conference, Brasil.

[6]. DNV, 2007, Recommended Practice RP O501 Erosive Wear in Piping Systems.

[7]. Forder, A., Thew, M., and Harrison, D., 1998, A numerical investigation of solid particle erosion experienced by oilfield control valves, Wear, 216, 184-193.

[8]. Guomei, L., Yueshe, W., Renyang, H., Xuewen, C., Changzhi, L., and Tao, M., 2009, Numerical simulation of predicting and reducing solid particle erosion of solid-liquid two-phase flow in a choke, Pet. Sci., 6, pp. 91-97.

[9]. Nguyen, V.B., Nguyen, Q.B., Liu, Z.G., Wan, S., Lim, C.Y.H., and Zhang, Y.W., 2014, A combined numerical experimental study on the effect of surface evolution on the water sand multiphase flow characteristics and the material erosion behavior, Wear, 319, pp. 96–109.

[10]. VV.AA., 1981, PHOENICS Encyclopedia. Available online at www.cham.co.uk.

[11]. Clift, R., Grace, J.R., and Weber, M.E., 1978, Bubbles, Drops and Particles. Academic Press, London and New York.

[12]. Gosman, A.D., Ioannides, E., 1981, Aspects of Computer Simulation of Liquid-Fueled Combustors, J. Energy, 7, pp. 482–490.

[13]. Spalding, D.B., 1980, Numerical computation of multiphase fluid flow and heat transfer, in: C. Taylor, K. Morgan (Eds.), Recent Advances in Numerical Methods in Fluids, Pineridge Press Limited, Swansea, UK, pp. 139-168.

[14]. Malavasi, S., and Messa, G.V., 2014, CFD modelling of a choke valve under critical working conditions, Proc. ASME 2014 Pressure Vessel and Piping Conference, 20-27 July 2014, Anaheim US-CA.

[15]. Launder, B.E., and Spalding, D.B., 1972, Mathematical models of turbulence, Academic Press, London and New York.

[16]. Spalding, D.B., 1972. A novel finite-difference formulation for differential expressions involving both first and second derivatives, Int. J. Numer. Meth. Eng., 4(4), pp. 551-559.

[17]. D.B. Spalding, 1980, Mathematical modelling of fluid mechanics, heat-transfer and chemical-reaction processes: a lecture course, CFDU Report HTS/80/1, Imperial College, London.

[18]. Okita, R., Zhang, Y., McLaury, B.S., and Shirazi, S.A., 2012, Experimental and Computational Investigations to Evaluate the Effects of Fluid Viscosity and Particle Size on Erosion Damage, ASME J. Fluids Eng., 134, No. 061301.